Chapter 5
Smart Fuzzy Fiber-Reinforced Piezoelectric Composites

Manas C. Ray

Abstract In this chapter analytical micromechanics model of a novel smart fuzzy fiber-reinforced composite (**SFFRC**) has been derived. The novel constructional feature of such **SFFRC** is that the existing vertically reinforced 1–3 piezoelectric composite has been hybridized by radially growing carbon nanotubes (**CNT**s) on the surface of the cylindrical vertical piezoelectric fibers. The model predicts that the effective in-plane piezoelectric coefficient and the elastic properties of such **SFFRC** are significantly improved over those of the existing 1–3 piezoelectric composite without reinforced with CNTs.

5.1 Piezoelectric Effects

Piezoelectric effect is an electromechanical coupling phenomenon exhibited by non-centrosymmetric dielectric materials. These materials do not possess inversion symmetry. This means that the inversion of the atomic positions alters the original crystalline structure, and different equilibrium positions of charges are associated with different polarization. Such polarization is called the piezoelectricity. Two types of piezoelectric effects exist in the piezoelectric materials. One of the effects by virtue of which the conversion of the mechanical energy into the electric energy occurs when the piezoelectric materials are deformed upon mechanical stimulus is called the direct piezoelectric effect. The other effect is called the converse piezoelectric effect by virtue of which piezoelectric materials are deformed due to the application of the electric field resulting in the conversion of the electrical energy into the mechanical energy. To exhibit piezoelectric effect, piezoelectric materials must be poled. Normally, a piezoelectric material has electric dipoles which are randomly oriented. When it is heated above a certain temperature called the Curie temperature and is subjected to a very strong electric field, the electric dipoles

M.C. Ray (✉)
Department of Mechanical Engineering, Indian Institute of Technology, Kharagpur 721302, India
e-mail: mcray@mech.iitkgp.ernet.in

S.A. Meguid (ed.), *Advances in Nanocomposites*,
DOI 10.1007/978-3-319-31662-8_5

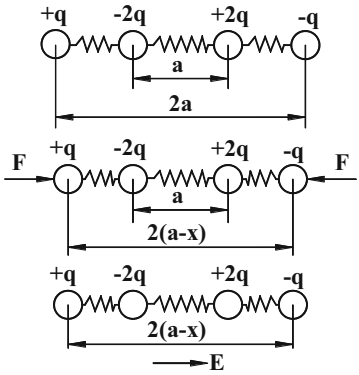

Fig. 5.1 Schematic representation of piezoelectric phenomena

reorient themselves and are aligned relative to the electric field. Such process is called poling. If the dipoles maintain their aligned orientations after cooling, the material is said to be poled and exhibits piezoelectric effect. Let four charges be in equilibrium on a straight line as shown in Fig. 5.1. Let the magnitudes of the first and the fourth charges be "$+q$" and "$-q$" while the second and the third charges be "$-2q$" and "$+2q$." The first and the fourth charges are "$2a$" apart, while the distance between the second and the third charges is "a." The locations of the charges are symmetric about the center, and thus, the charges are in equilibrium, but they are not centrosymmetric as the 180° rotation of this system of charges causes a different system of charges. The net dipole moment or the polarization of this system of charges is obviously zero. Now if the first and the fourth charges are displaced toward the center of the charges by an amount "x" due to an applied force F, this system of charges will exhibit a net polarization of amount "$2qx$." This displacement "x" is treated as the measure of mechanical deformation due to the application of mechanical energy. Thus the non-centrosymmetric system of charges exhibits electric polarization upon mechanical stimulation. On the other hand, if this system of charges is subjected to an electric field E, the charges will be displaced resulting in the conversion of the electrical energy into the mechanical energy.

5.2 Introduction to Smart Fuzzy Fiber-Reinforced Composite

In the quest for developing very lightweight high-performance flexible structures, a concept has emerged for developing the structures with self-controlling and/or self-monitoring capabilities. Expediently, utilizing the piezoelectric effects, Forward (1981) first attempted to demonstrate the feasibility of the effectiveness of the piezoelectric actuator to damp out the vibrations of a cylindrical fiber glass mast. Subsequently, Bailey and Hubbard (1985), (1987), Crawley and Luis (1987), and Im and Atluri (1989) successfully reported that the patches of piezoelectric

actuators being bonded with the host beams efficiently perform as the distributed actuators of the host beams. Miller and Hubbard (1987) first demonstrated that a layer of the piezoelectric material being integrated with a cantilever beam can act as the distributed sensor of the host cantilever beam. When these distributed sensors and actuators are coupled with the elements of the control systems such that the distributed piezoelectric actuators can be activated with a proper control voltage, the host structure attains the self-controlling and self-sensing capabilities. Such flexible host structures possessing built-in mechanism for achieving self-controlling and self-sensing capabilities are being customarily called as smart structures. Since its inception, enormous research (Baz and Poh 1988; Ha et al. 1992; Ray et al. 1994; Lin et al. 1996; Saravanos et al. 1997; Chee et al. 1999; Varadarajan et al. 2000; Ray and Pradhan 2007; Sohn et al. 2009; Ray and Faye 2009; Suresh Kumar and Ray 2012) on smart structures has been going on for developing very light weight smart flexible structures.

The performance of the smart structures depends on the magnitudes of the piezoelectric coefficients of the piezoelectric materials. The magnitudes of the piezoelectric coefficients of monolithic polymer piezoelectric materials are very low, while the monolithic piezoceramic materials are characterized with large values of the piezoelectric coefficients. But the monolithic piezoceramic materials such as **PZT5**, **PZT5H**, etc. are highly brittle and not conformable to the cylindrical surface or vibrating surface of the host structures. Hence, these smart materials find limitations in their use as distributed actuators. The conventional advanced fiber-reinforced composites are composed of brittle fibers of high stiffness. Probably this way of using high stiff brittle materials motivated the researchers to develop piezoelectric composites using brittle piezoceramic fibers. One of the commercially available piezoelectric composites (Smith and Auld 1991) is popularly known as 1–3 piezoelectric (**PZC**). In a lamina of vertically reinforced 1–3 **PZC**, the ceramic piezoelectric fibers are vertically aligned across the thickness of the lamina. Such 1–3 **PZC** provides a wide range of effective material properties not offered by the existing monolithic piezoelectric materials, renders anisotropic actuations, and is characterized by good conformability and strength. However, this 1–3 **PZC** also suffers from the drawback that its effective in-plane piezoelectric coefficient is much smaller than its transverse effective piezoelectric coefficient. The in-plane piezoelectric coefficient accounts for the performance of the piezoelectric actuator for bending control of smart structures. The performance of the distributed actuator made of such 1–3 **PZC** can be enhanced if the magnitude of its in-plane piezoelectric coefficient can be tailored to an improved value.

Since the discovery of carbon nanotubes (**CNT**s) (Iijima 1991), researchers have been carrying out extensive work (Treacy et al. 1996; Shen and Li 2004; Cheng et al. 2009) to predict their effective material properties, and it has been revealed that the **CNT**s are characterized with exceptionally high elastic properties. However, **CNT**s alone cannot be used for structural applications as they are difficult to be aligned and prone to agglomeration. To exploit the excellent elastic properties of **CNT**s, a great deal of research has been devoted to the development of high-performance nanocomposites using **CNT**s as reinforcements (Thostenson and

Chou 2003; Griebel and Hamaekers 2004; Odegard et al. 2003; Seidel and Lagoudas 2004; Jiang et al. 2009; Shadlou et al. 2011). For structural applications, recent research focuses on improving the effective properties of the existing advanced fiber-reinforced polymer composite by growing **CNT**s on the surfaces of the fiber reinforcements. Bower et al. (2000) demonstrated the growth of aligned **CNT**s on the substrate surface using microwave plasma-enhanced chemical vapor deposition. Mathur et al. (2008) experimentally investigated that the flexural strength and the modulus of the carbon fiber-reinforced composite can be improved by growing **CNT**s on the surface of the carbon fiber. Zhang et al. (2008) produced **CNT** arrays on the host aluminum silicate and the quartz fiber. Gracia et al. (2008) fabricated a hybrid laminate in which the reinforcement is a woven cloth of alumina fibers with in situ-grown **CNT**s on the surface of the fibers. They demonstrated that both the mechanical and electrical properties of such a laminate are enhanced because of **CNT**s grown on the surface of the alumina fibers. Recently, Kundalwal and Ray (2011, 2012) derived micromechanics models for estimating all the effective elastic coefficients of novel fuzzy fiber-reinforced composite (**FFRC**). Chatzigeorgiou et al. (2012) also estimated the effective mechanical properties of fuzzy fiber composite employing the composite cylinder method. Lanzara and Chang (2009) designed and fabricated the piezoelectric ceramic discs coated with vertically aligned **CNT**s. They demonstrated that the arrays of aligned **CNT**s can be normally grown on the surface of the piezoceramic (**PZT**) disc.

The paper authored by Lanzara and Chang (2009) motivated the author to presume that the **PZT** fibers may be coated with radially grown **CNT**s. Hence, in order to further improve the effective in-plane properties of the existing 1–3 **PZC**, Ray (2010) and Dhala and Ray (2015) delineated a concept of developing novel **SFFRC**. The **SFFRC** is a smart hybrid piezoelectric composite in which the piezoelectric fiber reinforcements are vertically aligned and **CNT**s are radially grown on the surfaces of these piezoelectric fibers. This chapter is concerned with the derivation of an analytical micromechanics model for estimating the effective elastic and piezoelectric properties of this novel **SFFRC**. First an analytical micromechanics model of the existing vertically reinforced 1–3 **PZC** is presented. How this model is augmented to derive the micromechanics model of **SFFRC** is presented in the subsequent sections. Numerical results are presented to demonstrate that the **CNT**s can improve the effective in-plane piezoelectric coefficient of the existing 1–3 **PZC**.

5.3 Three-Dimensional Effective Properties of 1–3 Piezoelectric Composites

Figure 5.2 schematically illustrates a lamina made of the vertically reinforced 1–3 piezoelectric composite (**PZC**). Here the pattern "1–3" refers to the connectivity pattern of the piezoelectric composite. In case of the pattern like "1–3," the first

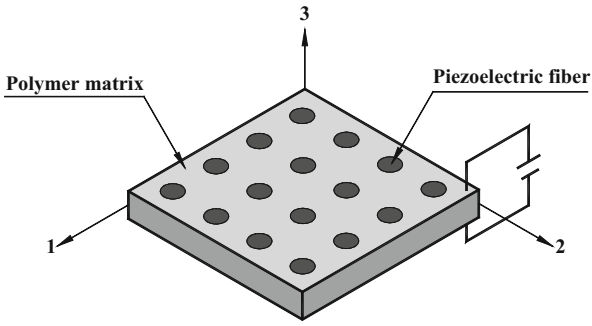

Fig. 5.2 Schematic diagram of a lamina of vertically reinforced 1–3 piezoelectric composite

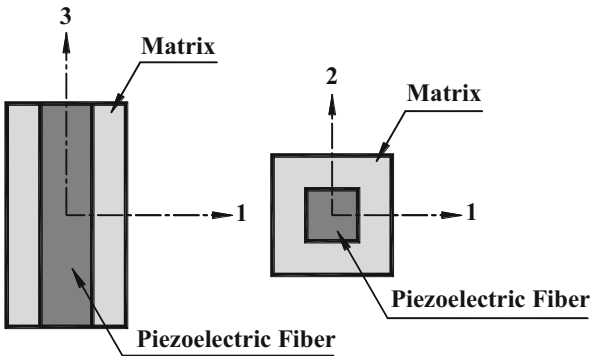

Fig. 5.3 In-plane and transverse cross sections of the RVE of the 1–3 piezoelectric composite

digit represents the number of connectivity of the fiber reinforcement along the principal material coordinate axes, while the second digit denotes the same of the matrix phase (Newnham et al. 1978). It may be observed from Fig. 5.2 that the piezoelectric fiber reinforcements are vertically aligned across the thickness of the lamina. The matrix phase is a polymer material.

The top and the bottom surfaces of the lamina are electroded such that the electric field can be applied across the thickness of the lamina. The orthogonal principal material coordinate system $(1-2-3)$ is considered in such a way that the 3-axis is aligned with the length of the fibers while 1- and 2-axes are aligned with the length and the width of the lamina, i.e., transverse to the fiber direction. The in-plane and vertical cross sections of the representative volume element (**RVE**) of this 1–3 **PZC** are illustrated in Fig. 5.3. It is considered that the lamina of the 1–3 **PZC** shown in Fig. 5.2 is subjected to the electric field along the thickness of the lamina only. Thus, the constitutive equations for the converse piezoelectric effect (Ray and Pradhan 2007), exhibited by the piezoelectric material of the fibers, are given by

$$\{\sigma^p\} = [C^p]\{\in^p\} - \{e^p\}E_3 \tag{5.1}$$

The constitutive relations for the matrix material are

$$\{\sigma^m\} = [C^m]\{\in^m\} \tag{5.2}$$

In Eqs. (5.1) and (5.2), $\{\sigma\}$, $\{\in\}$, and $[C]$ with superscript p or m represent the state of stress, the state of strain, and the elastic coefficient matrix at any point in the constituent phase, respectively, while $\{e\}$ and E_3 are the piezoelectric coefficient matrix and the electric field along the thickness (i.e., 3-axis) of the lamina of the 1–3 **PZC**, respectively. Their explicit forms are

$$\{\sigma^r\} = \begin{bmatrix}\sigma_1^r & \sigma_2^r & \sigma_3^r & \sigma_{23}^r & \sigma_{13}^r & \sigma_{12}^r\end{bmatrix}^T, \{\in^r\} = \begin{bmatrix}\in_1^r & \in_2^r & \in_3^r & \gamma_{23}^r & \gamma_{13}^r & \gamma_{12}^r\end{bmatrix}^T,$$

$$[C^r] = \begin{bmatrix} C_{11}^r & C_{12}^r & C_{13}^r & 0 & 0 & 0 \\ C_{12}^r & C_{22}^r & C_{23}^r & 0 & 0 & 0 \\ C_{13}^r & C_{23}^r & C_{33}^r & 0 & 0 & 0 \\ 0 & 0 & 0 & C_{44}^r & 0 & 0 \\ 0 & 0 & 0 & 0 & C_{55}^r & 0 \\ 0 & 0 & 0 & 0 & 0 & C_{66}^r \end{bmatrix} \text{and} \{e^p\} = \begin{Bmatrix} e_{31}^p \\ e_{32}^p \\ e_{33}^p \\ 0 \\ 0 \\ 0 \end{Bmatrix}; r = p \text{or} m \tag{5.3}$$

In Eq. (5.3), for the constituent phase denoted by r, σ_1^r, σ_2^r, and σ_3^r represent the normal stresses along the 1-, 2-, and 3-axes, respectively; σ_{23}^r, σ_{13}^r, and σ_{12}^r are the shear stresses; and C_{ij}^r is the elastic coefficient. Also, it may be noted that if the applied electric field is applied along the 3-direction, the in-plane piezoelectric coefficients e_{31}^p and e_{32}^p provide the measure of the in-plane actuations along the 1- and 2-directions, respectively, while the piezoelectric coefficient e_{33}^p accounts for the measure of the transverse actuation. The existence of perfect bonding between the fibers and the matrix phase in the **RVE** allows one to write the following iso-field conditions (Aboudi et al. 2013):

$$\begin{Bmatrix} \sigma_1^{pc} \\ \sigma_2^{pc} \\ \in_3^{pc} \\ \sigma_{23}^{pc} \\ \sigma_{13}^{pc} \\ \sigma_{12}^{pc} \end{Bmatrix} = \begin{Bmatrix} \sigma_1^m \\ \sigma_2^m \\ \in_3^m \\ \sigma_{23}^m \\ \sigma_{13}^m \\ \sigma_{12}^m \end{Bmatrix} = \begin{Bmatrix} \sigma_1^p \\ \sigma_2^p \\ \in_3^p \\ \sigma_{23}^p \\ \sigma_{13}^p \\ \sigma_{12}^p \end{Bmatrix} \tag{5.4}$$

The existence of perfect bonding between the fibers and matrix also requires to satisfy the following rules of mixtures (Aboudi et al. 2013):

$$\begin{aligned} &\sigma_3^{pc} = V_p\sigma_3^p + V_m\sigma_3^m,\ \in_1^{pc} = V_p \in_1^p + V_m \in_1^m,\ \in_2^{pc} = V_p \in_2^p + V_m \in_2^m, \\ &\gamma_{23}^{pc} = V_p\gamma_{23}^p + V_m\gamma_{23}^m, \gamma_{13}^{pc} = V_p\gamma_{13}^p + V_m\gamma_{13}^m, \gamma_{12}^{pc} = V_p\gamma_{12}^p + V_m\gamma_{12}^m, \end{aligned} \tag{5.5}$$

In Eq. (5.5), V_p and V_m represent the piezoelectric fiber volume fraction and the matrix volume fraction in the **RVE** of the 1–3 **PZC**, respectively. It should be noted that the field variables with superscript *pc* appearing in Eqs. (5.4) and (5.5) represent the field variables of the homogenized **RVE** of the 1–3 **PZC**. At this juncture, it must be noted that a field variable used here for the constituent phases or the homogenized **RVE** actually represents the average of the corresponding field variable in the constituent phases or the homogenized **RVE**, respectively (Aboudi et al. 2013). The state of stress $\{\sigma^{pc}\}$ and the state of strain $\{\in^{pc}\}$ in the homogenized **RVE** can be written in terms of the strains in the constituent phases as follows:

$$\{\sigma^{pc}\} = [C_1]\{\in^p\} + [C_2]\{\in^m\} - \{e_1\}\{E\} \tag{5.6}$$

$$\{\in^{pc}\} = [V_1]\{\in^p\} + [V_2]\{\in^m\} \tag{5.7}$$

in which

$$\{\sigma^{pc}\} = \begin{Bmatrix} \sigma_1^{pc} \\ \sigma_2^{pc} \\ \sigma_3^{pc} \\ \sigma_{23}^{pc} \\ \sigma_{13}^{pc} \\ \sigma_{12}^{pc} \end{Bmatrix}, \{\in^{pc}\} = \begin{Bmatrix} \in_1^{pc} \\ \in_2^{pc} \\ \in_3^{pc} \\ \gamma_{23}^{pc} \\ \gamma_{13}^{pc} \\ \gamma_{12}^{pc} \end{Bmatrix}, [C_1] = \begin{bmatrix} 0 & 0 & 0 & 0 & 0 & 0 \\ 0 & 0 & 0 & 0 & 0 & 0 \\ V_p C_{13}^p & V_p C_{23}^p & V_p C_{33}^p & 0 & 0 & 0 \\ 0 & 0 & 0 & 0 & 0 & 0 \\ 0 & 0 & 0 & 0 & 0 & 0 \\ 0 & 0 & 0 & 0 & 0 & 0 \end{bmatrix}$$

$$[C_2] = \begin{bmatrix} C_{11}^m & C_{12}^m & C_{13}^m & 0 & 0 & 0 \\ C_{12}^m & C_{22}^m & C_{23}^m & 0 & 0 & 0 \\ V_m C_{13}^m & V_m C_{23}^m & V_m C_{33}^m & 0 & 0 & 0 \\ 0 & 0 & 0 & C_{44}^m & 0 & 0 \\ 0 & 0 & 0 & 0 & C_{55}^m & 0 \\ 0 & 0 & 0 & 0 & 0 & C_{66}^m \end{bmatrix}, \{e_1\} = \begin{Bmatrix} 0 \\ 0 \\ V_p e_{33}^p \\ 0 \\ 0 \\ 0 \end{Bmatrix}$$

$$[V_1] = \begin{bmatrix} V_p & 0 & 0 & 0 & 0 & 0 \\ 0 & V_p & 0 & 0 & 0 & 0 \\ 0 & 0 & 1 & 0 & 0 & 0 \\ 0 & 0 & 0 & V_p & 0 & 0 \\ 0 & 0 & 0 & 0 & V_p & 0 \\ 0 & 0 & 0 & 0 & 0 & V_p \end{bmatrix} \text{ and } [V_2] = \begin{bmatrix} V_m & 0 & 0 & 0 & 0 & 0 \\ 0 & V_m & 0 & 0 & 0 & 0 \\ 0 & 0 & 0 & 0 & 0 & 0 \\ 0 & 0 & 0 & V_m & 0 & 0 \\ 0 & 0 & 0 & 0 & V_m & 0 \\ 0 & 0 & 0 & 0 & 0 & V_m \end{bmatrix} \tag{5.8}$$

The continuity conditions between the fiber and the matrix phase of the **RVE** of the 1–3 **PZC** given in Eq. (5.4) can be expressed in terms of the strains in the constituent phases and the electric field as follows:

$$[C_3]\{\in^p\} - [C_4]\{\in^m\} = \{e_2\}\{E\} \tag{5.9}$$

in which

$$[C_3] = \begin{bmatrix} C_{11}^p & C_{12}^p & C_{13}^p & 0 & 0 & 0 \\ C_{12}^p & C_{22}^p & C_{23}^p & 0 & 0 & 0 \\ 0 & 0 & 1 & 0 & 0 & 0 \\ 0 & 0 & 0 & C_{44}^p & 0 & 0 \\ 0 & 0 & 0 & 0 & C_{55}^p & 0 \\ 0 & 0 & 0 & 0 & 0 & C_{66}^p \end{bmatrix}, [C_4] = \begin{bmatrix} C_{11}^m & C_{12}^m & C_{13}^m & 0 & 0 & 0 \\ C_{12}^m & C_{22}^m & C_{23}^m & 0 & 0 & 0 \\ 0 & 0 & 1 & 0 & 0 & 0 \\ 0 & 0 & 0 & C_{44}^m & 0 & 0 \\ 0 & 0 & 0 & 0 & C_{55}^m & 0 \\ 0 & 0 & 0 & 0 & 0 & C_{66}^m \end{bmatrix},$$

$$\text{and } \{e_2\} = \begin{bmatrix} e_{31}^p & e_{32}^p & 0 & 0 & 0 & 0 \end{bmatrix}^T \tag{5.10}$$

Using Eqs. (5.6) and (5.8), one can derive that

$$\{\in^m\} = [V_3]^{-1}\{\in^{pc}\} - [V_3]^{-1}[V_1][C_3]^{-1}\{e_2\}E_3 \tag{5.11}$$

and

$$\{\in^p\} = [V_4]^{-1}\{\in^{pc}\} - [V_4]^{-1}[V_2][C_4]^{-1}\{e_2\}E_3 \tag{5.12}$$

in which

$[V_3] = [V_2] + [V_1][C_3]^{-1}[C_4]$ and $[V_4] = [V_1] + [V_2][C_4]^{-1}[C_3]$.

Substituting Eqs. (5.10) and (5.11) into Eq. (5.5), the following effective constitutive relation for the converse piezoelectric effect in the vertically reinforced 1–3 **PZC** can be derived:

$$\{\sigma^{pc}\} = [C^{pc}]\{\in^{pc}\} - \{e^{pc}\}E_3 \tag{5.13}$$

in which the effective elastic coefficient matrix $[C^{pc}]$ and the effective piezoelectric coefficient matrix $\{e^{pc}\}$ of the 1–3 **PZC** are given by

$$[C^{pc}] = [C_1][V_4]^{-1} + [C_2][V_3]^{-1} \tag{5.14}$$

$$\{e^{pc}\} = \{e_1\} - [C_1][V_4]^{-1}[V_2][C_4]^{-1}\{e_2\} + [C_2][V_3]^{-1}[V_1][C_3]^{-1}\{e_2\} \tag{5.15}$$

It is obvious from Eq. (5.14) that the in-plane effective piezoelectric coefficients e_{31}^{pc} and e_{32}^{pc} of the 1–3 **PZC** are $e^{pc}(1)$ and $e^{pc}(2)$, respectively, while the transverse

effective piezoelectric coefficient e_{33}^{pc} of the 1–3 **PZC** is $e^{pc}(3)$. It may be noted that the matrix $[C_4]$ contains the elastic properties of the matrix phase. Hence, it is obvious from the expression of the effective piezoelectric coefficient $\{e^{pc}\}$ given by Eq. (5.14) that for a particular piezoelectric material, the magnitude of the effective piezoelectric coefficient can be improved if the elastic properties of the matrix are improved.

5.4 Effective Properties of the SFFRC

Figure 5.4 illustrates a schematic sketch of a lamina of the **SFFRC**. The novel constructional feature of such a continuous unidirectional vertically reinforced composite is that **CNT**s of equal length are uniformly aligned in the plane of the lamina and radially grown on the surface of the piezoelectric fiber reinforcements. **CNT**s considered here are transversely isotropic (Shen and Li 2004). They are grown on the surface of the piezoelectric fibers in such a way that their axes of transverse isotropy are normal to the surface of the piezoelectric fibers. Such a resulting piezoelectric fuzzy fiber (**PFF**) is shown in Fig. 5.5. When this **PFF** is embedded into the polymer material, the gap between the **CNT**s is filled with the polymer. Therefore, the radially aligned **CNT**s reinforce the polymer matrix surrounding the piezoelectric fiber along the direction transverse to the length of the piezoelectric fiber. Consequently, the augmented **PFF** can be viewed as a circular cylindrical piezoelectric composite fuzzy fiber (**PCFF**) in which a piezoelectric fiber is embedded in the **CNT**-reinforced polymer matrix nanocomposite (**PMNC**) and the radius of the **PCFF** is equal to the sum of the radius of the piezoelectric fiber and the length of a **CNT**. The cross sections of such a **PCFF** are illustrated in Fig. 5.6. Therefore, the **RVE** of the **SFFRC** can be treated as being composed of two phases where the reinforcement is the **PCFF** and the matrix is the polymer material. The piezoelectric fiber is poled along the thickness direction, and the only electric field considered here is applied across the thickness of the lamina. Thus, the analytical micromechanics model for estimating the effective properties of the

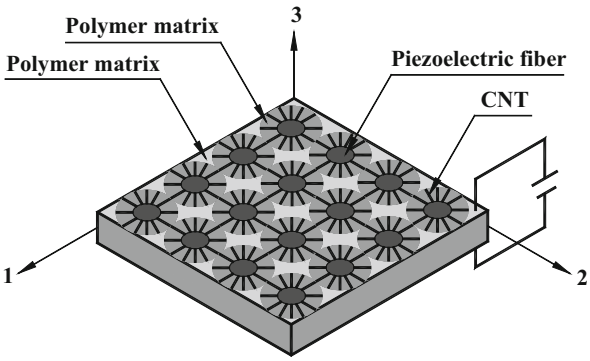

Fig. 5.4 Schematic diagram of a lamina of smart fuzzy fiber-reinforced composite (SFFRC)

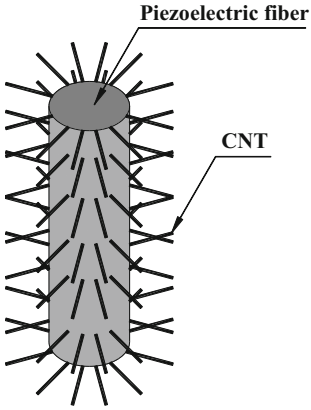

Fig. 5.5 Piezoelectric fuzzy fiber (**PFF**)

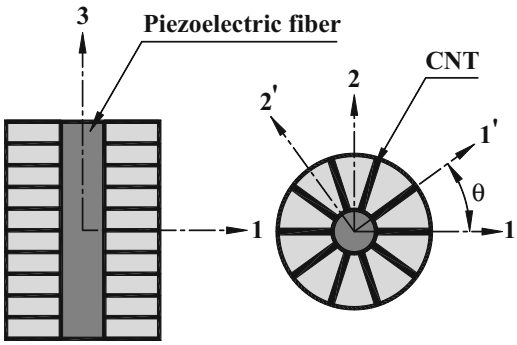

Fig. 5.6 Longitudinal and transverse cross sections

SFFRC first needs the derivation of the micromechanics model for estimating the effective elastic properties of the **PMNC** material. Subsequently, considering the **PMNC** material as the matrix phase and the piezoelectric fibers as the reinforcements, effective elastic properties and effective piezoelectric properties of the **PCFF** are to be computed. Finally, utilizing the effective properties of the **PCFF** and the polymer matrix, the effective properties of the **SFFRC** can be estimated. Also, **PCFF**s are assumed to be uniformly spaced over the volume of a lamina of the **SFFRC** in such a way that three orthogonal principal material coordinate axes (1–2–3) exist in the composite as shown in Fig. 5.4. Micromechanics models for estimating the properties of the **PMNC**, the **PCFF**, and the **SFFRC** are derived in the following sections.

5.4.1 Micromechanics Model of the PMNC

This section presents a simple micromechanics model to estimate the effective elastic properties of the **PMNC** material surrounding the piezoelectric fiber which

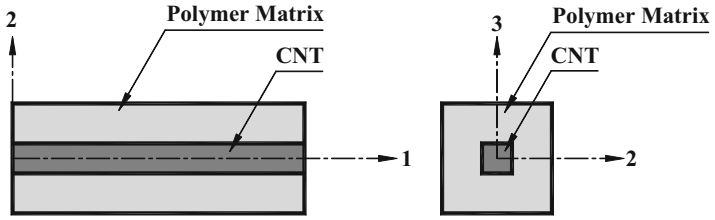

Fig. 5.7 Longitudinal and transverse section of the **RVE** of the **PMNC**

are required as inputs for the derivation of the model of the **PCFF**. Since the piezoelectric fibers are vertically aligned, the radially grown **CNT**s on the surface of the piezoelectric fibers are aligned either with the 1-axis or with the $1'$-axis as shown in Fig. 5.6. Let us first estimate the properties of an **RVE** in which the **CNT** fiber aligns with the 1-axis. The cross sections of such an **RVE** of the **PMNC** have been shown in Fig. 5.7. Assuming **CNTs** as solid fibers (Gao and Li 2005), the micromechanics model derived in Sect. 5.3 can be modified to predict the average effective elastic constants of the **PMNC** surrounding the piezoelectric fiber. Based on the principal material coordinate (1–2–3) axes shown in Fig. 5.7, the constitutive relations for the constituent phases of the **RVE** of the **PMNC** are given by

$$\{\sigma^r\} = [C^r]\{\in^r\};\ r = nt \,\text{and}\, m \tag{5.16}$$

where the stress vector, the strain vector, and the elastic coefficient matrix of the phase denoted by r are given by Eq. (5.3). In Eq. (5.14) the superscripts nt and m denote, respectively, the **CNT** fiber and the monolithic polymer matrix. It may be mentioned here that the basics of **CNT**s may be studied from some original literature (Thostenson and Chou 2003). It is assumed that **CNTs** and the polymer matrix are perfectly bonded. Therefore, the following iso-field relations and the rules of mixture (Aboudi et al. 2013) satisfying the perfect bonding conditions between the fiber and the matrix can be written as

$$\begin{Bmatrix} \sigma_2^{nc} \\ \sigma_3^{nc} \\ \in_1^{nc} \\ \sigma_{23}^{nc} \\ \sigma_{13}^{nc} \\ \sigma_{12}^{nc} \end{Bmatrix} = \begin{Bmatrix} \sigma_2^{m} \\ \sigma_3^{m} \\ \in_1^{m} \\ \sigma_{23}^{m} \\ \sigma_{13}^{m} \\ \sigma_{12}^{m} \end{Bmatrix} = \begin{Bmatrix} \sigma_2^{nt} \\ \sigma_3^{nt} \\ \in_1^{nt} \\ \sigma_{23}^{nt} \\ \sigma_{13}^{nt} \\ \sigma_{12}^{nt} \end{Bmatrix} \tag{5.17}$$

and

$$\begin{aligned} &\sigma_1^{nc} = V_{nt}\sigma_1^{nt} + V_m\sigma_1^{nt},\ \in_2^{nc} = V_{nt}\in_2^{nt} + V_m\in_2^{m},\ \in_3^{nc} = V_{nt}\in_3^{nt} + V_m\in_3^{m},\\ &\gamma_{23}^{nc} = V_{nt}\gamma_{23}^{nt} + V_m\gamma_{23}^{m},\ \gamma_{13}^{nc} = V_{nt}\gamma_{13}^{nt} + V_m\gamma_{13}^{m} \text{ and } \gamma_{12}^{nc} = V_{nt}\gamma_{12}^{nt} + V_m\gamma_{12}^{m} \end{aligned} \tag{5.18}$$

In Eqs. (5.15) and (5.17), V_{nt} is the volume fraction of the **CNT** with respect to the volume of the **RVE** of the **PMNC** and $V_m = 1 - V_{nt}$. Also, the superscript nc represents the homogenized **PMNC** material. From Eqs. (5.15) and (5.17), the stress and the strain vectors in the homogenized **PMNC** material can be expressed in terms of the strain vectors of the constituent phases as follows:

$$\{\sigma^{nc}\} = [C_5]\{\in^{nt}\} + [C_6]\{\in^{m}\} \tag{5.19}$$

$$\{\in^{nc}\} = [V_5]\{\in^{nt}\} + [V_6]\{\in^{m}\} \tag{5.20}$$

Also, using the iso-field conditions between the constituent phases given by Eq. (5.15), the relations among the strains in the constituent phases can be written as

$$[C_7]\{\in^{nt}\} = [C_8]\{\in^{m}\} \tag{5.21}$$

The various matrices appearing in Eqs. (5.16)–(5.18) are

$$[C_5] = V_{nt}\begin{bmatrix} C_{11}^{nt} & C_{12}^{nt} & C_{13}^{nt} & 0 & 0 & 0 \\ 0 & 0 & 0 & 0 & 0 & 0 \\ 0 & 0 & 0 & 0 & 0 & 0 \\ 0 & 0 & 0 & 0 & 0 & 0 \\ 0 & 0 & 0 & 0 & 0 & 0 \\ 0 & 0 & 0 & 0 & 0 & 0 \end{bmatrix}, [C_6] = \begin{bmatrix} V_m C_{11}^{m} & V_m C_{12}^{m} & V_m C_{13}^{m} & 0 & 0 & 0 \\ C_{12}^{m} & C_{22}^{m} & C_{23}^{m} & 0 & 0 & 0 \\ C_{13}^{m} & C_{23}^{m} & C_{33}^{m} & 0 & 0 & 0 \\ 0 & 0 & 0 & 0 & 0 & 0 \\ 0 & 0 & 0 & 0 & 0 & 0 \\ 0 & 0 & 0 & 0 & 0 & 0 \end{bmatrix},$$

$$[V_5] = \begin{bmatrix} 1 & 0 & 0 & 0 & 0 & 0 \\ 0 & V_{nt} & 0 & 0 & 0 & 0 \\ 0 & 0 & V_{nt} & 0 & 0 & 0 \\ 0 & 0 & 0 & V_{nt} & 0 & 0 \\ 0 & 0 & 0 & 0 & V_{nt} & 0 \\ 0 & 0 & 0 & 0 & 0 & V_{nt} \end{bmatrix}, [V_6] = \begin{bmatrix} 0 & 0 & 0 & 0 & 0 & 0 \\ 0 & V_m & 0 & 0 & 0 & 0 \\ 0 & 0 & V_m & 0 & 0 & 0 \\ 0 & 0 & 0 & V_m & 0 & 0 \\ 0 & 0 & 0 & 0 & V_m & 0 \\ 0 & 0 & 0 & 0 & 0 & V_m \end{bmatrix},$$

$$[C_7] = \begin{bmatrix} 1 & 0 & 0 & 0 & 0 & 0 \\ C_{12}^{nt} & C_{22}^{nt} & C_{23}^{nt} & 0 & 0 & 0 \\ C_{13}^{nt} & C_{23}^{nt} & C_{33}^{nt} & 0 & 0 & 0 \\ 0 & 0 & 0 & C_{44}^{nt} & 0 & 0 \\ 0 & 0 & 0 & 0 & C_{55}^{nt} & 0 \\ 0 & 0 & 0 & 0 & 0 & C_{66}^{nt} \end{bmatrix}, [C_8] = \begin{bmatrix} 1 & 0 & 0 & 0 & 0 & 0 \\ C_{12}^{m} & C_{22}^{m} & C_{23}^{m} & 0 & 0 & 0 \\ C_{13}^{m} & C_{23}^{m} & C_{33}^{m} & 0 & 0 & 0 \\ 0 & 0 & 0 & C_{44}^{m} & 0 & 0 \\ 0 & 0 & 0 & 0 & C_{55}^{m} & 0 \\ 0 & 0 & 0 & 0 & 0 & C_{66}^{m} \end{bmatrix}, \tag{5.22}$$

Using Eqs. (5.17) and (5.18), the local strain vectors $\{\in^{nt}\}$ and $\{\in^{m}\}$ can be expressed in terms of $\{\in^{nc}\}$, and subsequently, using them in Eq. (5.16), the following constitutive relation between the states of stresses and strains at any point in the homogenized **PMNC** material is obtained:

$$\{\sigma^{nc}\} = [C^{nc}]\{\in^{nc}\} \tag{5.23}$$

where the effective elastic coefficient matrix $[C^{nc}]$ of the lamina of the **PMNC** is given by

$$[C^{nc}] = [C_5][V_8]^{-1} + [C_6][V_7]^{-1} \tag{5.24}$$

in which

$$[V_7] = [V_6] + [V_5][C_7]^{-1}[C_8] \text{ and } [V_8] = [V_5] + [V_6][C_8]^{-1}[C_7] \tag{5.25}$$

It should be noted that the effective elastic coefficient matrix at a point in the portion of the **PMNC** surrounding the piezoelectric fiber where the **CNT** is aligned with the 1-axis or $1'$-axis is given by $[C^{nc}]$. Thus, the matrix $[C^{nc}]$ provides the local effective elastic coefficient matrix at a point in the **PMNC** either with respect to the $1-2-3$ coordinate system or with respect to the $1^{'}-2^{'}-3$ coordinate system. But for estimating the effective properties of the **SFFRC**, the homogenized properties of the **PMNC** with respect to the $1-2-3$ coordinate system are to be estimated. For the point located in the **PMNC** where the **CNT** is oriented at an angle θ with the 1-axis of the $1-2$ plane, the effective elastic coefficient matrix $\left[\overline{C}^{nc}\right]$ at the said point with respect to the $1-2-3$ coordinate system can be obtained by the following transformations:

$$\left[\overline{C}^{nc}\right] = [T]^{T}[C^{nc}][T] \tag{5.26}$$

where

$$[T] = \begin{bmatrix} m^2 & n^2 & 0 & 0 & 0 & -2mn \\ n^2 & m^2 & 0 & 0 & 0 & 2mn \\ 0 & 0 & 1 & 0 & 0 & 0 \\ 0 & 0 & 0 & m & n & 0 \\ 0 & 0 & 0 & -n & m & 0 \\ mn & -mn & 0 & 0 & 0 & m^2 - n^2 \end{bmatrix}, m = \cos\theta \text{ and } n = \sin\theta \tag{5.27}$$

Therefore, the effective elastic properties of the **PMNC** surrounding the piezoelectric fiber with respect to the principal material coordinate axes of the **SFFRC** varies over an annular cross section of the **PMNC** phase of the **RVE** of the **PCFF**. However, without loss of generality, the volume average of these location-dependent effective

elastic properties $\left[\overline{C}^{nc}\right]$ over the volume of the **PMNC** can be treated as the effective elastic properties $[C^{\text{PMNC}}]$ of the **PMNC** material surrounding the piezoelectric fiber with respect to the 1–2–3 coordinate axes of the **SFFRC** and is given by

$$\left[C^{\text{PMNC}}\right] = \frac{1}{\pi\left(R^2 - a^2\right)} \int_0^{2\pi} \int_a^R \overline{C}^{nc} r \, dr \, d\theta \tag{5.28}$$

in which a and R are the radii of the piezoelectric fiber and the **PCFF**, respectively. Thus, the effective constitutive relations for the **PMNC** material with respect to the principal material coordinate axes of the **SFFRC** can be expressed as

$$\left\{\sigma^{\text{PMNC}}\right\} = \left[C^{\text{PMNC}}\right]\left\{\in^{\text{PMNC}}\right\} \tag{5.29}$$

5.4.2 *Effective Elastic Properties of the PCFF*

The constructional feature of the **PCFF** shown in Fig. 5.6 can be viewed as a circular cylindrical fiber which has been cut from a lamina of the vertically reinforced 1–3 **PZC**. The reinforcement phase of such 1–3 **PZC** is the piezoelectric fiber and the matrix phase is composed of the homogenized **PMNC** material with its effective elastic properties given by Eq. (5.23). Thus, following the micromechanics model derived in Sect. 5.3 for the vertically reinforced 1–3 **PZC**, the constitutive relation for the converse piezoelectric effect in the **PCFF** can be derived as follows:

$$\left\{\sigma^{\text{PCFF}}\right\} = \left[C^{\text{PCFF}}\right]\left\{\in^{\text{PCFF}}\right\} - \left\{e^{\text{PCFF}}\right\}E_3 \tag{5.30}$$

in which the effective elastic coefficient matrix $[C^{\text{PCFF}}]$ and the effective piezoelectric coefficient matrix $\{e^{\text{PCFF}}\}$ of the **PCFF** are

$$\left[C^{\text{PCFF}}\right] = [C_9][V_{12}]^{-1} + [C_{10}][V_{11}]^{-1} \tag{5.31}$$

$$\left\{e^{\text{PCFF}}\right\} = \{e_1\} - [C_9][V_{12}]^{-1}[V_{10}][C_{12}]^{-1}\{e_2\} + [C_{10}][V_{11}]^{-1}[V_9][C_{11}]^{-1}\{e_2\} \tag{5.32}$$

The various matrices appearing in Eqs. (5.26) and (5.27) are

$$[C_9] = [C_1],\ [C_{11}] = [C_3],$$

$$[C_{10}] = \begin{bmatrix} C_{11}^{\text{PMNC}} & C_{12}^{\text{PMNC}} & C_{13}^{\text{PMNC}} & 0 & 0 & 0 \\ C_{12}^{\text{PMNC}} & C_{22}^{\text{PMNC}} & C_{23}^{\text{PMNC}} & 0 & 0 & 0 \\ V_{\text{PMNC}}C_{13}^{\text{PMNC}} & V_{\text{PMNC}}C_{23}^{\text{PMNC}} & V_{\text{PMNC}}C_{33}^{\text{PMNC}} & 0 & 0 & 0 \\ 0 & 0 & 0 & C_{44}^{\text{PMNC}} & 0 & 0 \\ 0 & 0 & 0 & 0 & C_{55}^{\text{PMNC}} & 0 \\ 0 & 0 & 0 & 0 & 0 & C_{66}^{\text{PMNC}} \end{bmatrix},$$

$$[V_9] = \begin{bmatrix} \overline{V}_p & 0 & 0 & 0 & 0 & 0 \\ 0 & \overline{V}_p & 0 & 0 & 0 & 0 \\ 0 & 0 & 1 & 0 & 0 & 0 \\ 0 & 0 & 0 & \overline{V}_p & 0 & 0 \\ 0 & 0 & 0 & 0 & \overline{V}_p & 0 \\ 0 & 0 & 0 & 0 & 0 & \overline{V}_p \end{bmatrix},$$

$$[V_{10}] = \begin{bmatrix} V_{\text{PMNC}} & 0 & 0 & 0 & 0 & 0 \\ 0 & V_{\text{PMNC}} & 0 & 0 & 0 & 0 \\ 0 & 0 & 0 & 0 & 0 & 0 \\ 0 & 0 & 0 & V_{\text{PMNC}} & 0 & 0 \\ 0 & 0 & 0 & 0 & V_{\text{PMNC}} & 0 \\ 0 & 0 & 0 & 0 & 0 & V_{\text{PMNC}} \end{bmatrix},$$

$$[C_{12}] = \begin{bmatrix} C_{11}^{\text{PMNC}} & C_{12}^{\text{PMNC}} & C_{13}^{\text{PMNC}} & 0 & 0 & 0 \\ C_{12}^{\text{PMNC}} & C_{22}^{\text{PMNC}} & C_{23}^{\text{PMNC}} & 0 & 0 & 0 \\ 0 & 0 & 1 & 0 & 0 & 0 \\ 0 & 0 & 0 & C_{44}^{\text{PMNC}} & 0 & 0 \\ 0 & 0 & 0 & 0 & C_{55}^{\text{PMNC}} & 0 \\ 0 & 0 & 0 & 0 & 0 & C_{66}^{\text{PMNC}} \end{bmatrix},$$

$$V_{\text{PMNC}} = 1 - \overline{V}_p,\ [V_{11}] = [V_{10}] + [V_9][C_{11}]^{-1}[C_{12}]$$

$$\text{and}\ \ [V_{12}] = [V_9] + [V_{10}][C_{12}]^{-1}[C_{11}] \tag{5.33}$$

It should be noted that here the piezoelectric fiber volume fraction $\overline{V}_p$ is based on the volume of the **RVE** of the **PCFF**.

5.4.3 *Effective Properties of the SFFRC*

The constructional feature of the **SFFRC** can also be viewed as a vertically reinforced 1–3 **PZC** in which the **PCFF** is the piezoelectric fiber reinforcement and the monolithic polymer is the matrix phase. Thus, replacing the piezoelectric fiber by the **PCFF** in the micromechanics model of the 1–3 **PZC** derived in Sect. 5.3, the micromechanics model of the converse piezoelectric effect in the **SFFRC** can be derived as follows:

$$\{\sigma\} = [C]\{\in\} - \{e\}E_3 \tag{5.34}$$

in which the effective elastic coefficient matrix $[C]$ and the effective piezoelectric coefficient matrix $\{e\}$ of the **SFFRC** are given by

$$[C] = [C_{13}][V_{16}]^{-1} + [C_{14}][V_{15}]^{-1} \tag{5.35}$$

$$\{e\} = \{e_3\} - [C_{13}][V_{16}]^{-1}[V_{14}][C_{16}]^{-1}\{e_4\} + [C_{14}][V_{15}]^{-1}[V_{13}][C_{15}]^{-1}\{e_4\} \tag{5.36}$$

The various matrices appearing in Eqs. (5.30) and (5.31) are

$$[C_{13}] = V_{\text{PCFF}}\begin{bmatrix} 0 & 0 & 0 & 0 & 0 & 0 \\ 0 & 0 & 0 & 0 & 0 & 0 \\ C_{13}^{\text{PCFF}} & C_{23}^{\text{PCFF}} & C_{33}^{\text{PCFF}} & 0 & 0 & 0 \\ 0 & 0 & 0 & 0 & 0 & 0 \\ 0 & 0 & 0 & 0 & 0 & 0 \\ 0 & 0 & 0 & 0 & 0 & 0 \end{bmatrix}, [C_{14}] = [C_2], [V_{14}] = [V_2],$$

$$[V_{13}] = \begin{bmatrix} V_{\text{PCFF}} & 0 & 0 & 0 & 0 & 0 \\ 0 & V_{\text{PCFF}} & 0 & 0 & 0 & 0 \\ 0 & 0 & 1 & 0 & 0 & 0 \\ 0 & 0 & 0 & V_{\text{PCFF}} & 0 & 0 \\ 0 & 0 & 0 & 0 & V_{\text{PCFF}} & 0 \\ 0 & 0 & 0 & 0 & 0 & V_{\text{PCFF}} \end{bmatrix},$$

$$[V_{15}] = [V_{14}] + [V_{13}][C_{15}]^{-1}[C_{16}], [V_{16}] = [V_{13}] + [V_{14}][C_{16}]^{-1}[C_{15}],$$

$$[C_{15}] = \begin{bmatrix} C_{11}^{\text{PCFF}} & C_{12}^{\text{PCFF}} & C_{13}^{\text{PCFF}} & 0 & 0 & 0 \\ C_{12}^{\text{PCFF}} & C_{22}^{\text{PCFF}} & C_{23}^{\text{PCFF}} & 0 & 0 & 0 \\ 0 & 0 & 1 & 0 & 0 & 0 \\ 0 & 0 & 0 & C_{44}^{\text{PCFF}} & 0 & 0 \\ 0 & 0 & 0 & 0 & C_{55}^{\text{PCFF}} & 0 \\ 0 & 0 & 0 & 0 & 0 & C_{66}^{\text{PCFF}} \end{bmatrix}, [C_{16}] = [C_4],$$

$$\{e_3\} = \begin{bmatrix} 0 & 0 & V_{\text{PCFF}}e_{33}^{\text{PCFF}} & 0 & 0 & 0 \end{bmatrix}^T \text{and} \{e_4\} = \begin{bmatrix} e_{31}^{\text{PCFF}} & e_{32}^{\text{PCFF}} & 0 & 0 & 0 & 0 \end{bmatrix}^T \tag{5.37}$$

5.5 Determination of Volume Fractions

Volume fraction of **CNT**s (V_{CNT}) in the **SFFRC** depends on the **CNT** diameter, the piezoelectric fiber diameter, and the surface to surface distance of two adjacent radially aligned **CNT**s at their roots. The surface to surface distance between the two adjacent **CNT**s at their roots is considered as 1.7 nm (Jiang et al. 2009). For fibers with circular cross section, it is well known that the hexagonal array of packing is the optimal packing of fibers and the corresponding maximum fiber volume fraction is 0.9069. Hence, for computing the numerical values of the effective properties of the **SFFRC**, the hexagonal packing array of the **PCFF**s is considered as shown in Fig. 5.8. It is also to be noted that the number of **CNT**s grown on the surface of the piezoelectric fibers imposes a constraint on the maximum value of V_{CNT}. Thus, one cannot arbitrarily assume the large value of V_{CNT}. Based on the hexagonal array of packing of the **PCFF**, the transverse cross section of the **RVE** of the **SFFRC** will be an equilateral triangle. Thus, the volume (V^{SFFRC}) of the **RVE** of the **SFFRC** is given by

$$V^{\mathrm{SFFRC}} = \frac{\sqrt{3}}{4} D^2 L \tag{5.38}$$

where D is the diameter of the **PCFF** and L is the length of the **RVE**. The volume (V^p) of the piezoelectric fiber is

$$V^p = \frac{\pi}{8} d^2 L \tag{5.39}$$

where d is the diameter of the piezoelectric fiber. Thus, the piezoelectric fiber volume fraction (V_p) in the **SFFRC** can be found as

$$V_p = \frac{V^p}{V^{\mathrm{SFFRC}}} = \frac{\pi}{2\sqrt{3}} \frac{d^2}{D^2} \tag{5.40}$$

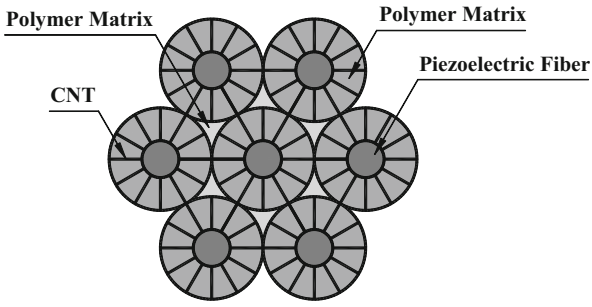

Fig. 5.8 Hexagonal array of packing for the **PCFF** fibers in **SFFRC**

Using Eqs. (5.34) and (5.35), the piezoelectric fiber volume fraction ($\overline{V}_p$) based on the volume of the **PCFF** can be determined as

$$\overline{V}_p = \frac{2\sqrt{3}}{\pi} V_p \tag{5.41}$$

Based on the surface to surface distance at the roots of the two adjacent **CNT**s and the **CNT** diameter, the maximum number of radially grown aligned **CNT**s ($N_{\text{CNT}}|_{\max}$) on the surface of the piezoelectric fiber can be determined as

$$N_{\text{CNT}}|_{\max} = \frac{\pi dL}{2\left(d_n + 1.7 \times 10^{-9}\right)^2} \tag{5.42}$$

where d_n is the diameter of **CNT**. Therefore, the volume of **CNT**s (V^{CNT}) present in the **RVE** is

$$V^{\text{CNT}} = \frac{\pi}{\pi} d_n^2 (R - a) N_{\text{CNT}}|_{\max} \tag{5.43}$$

Thus, the maximum volume fraction ($V_{\text{CNT}}|_{\max}$) of **CNT**s with respect to the volume of the **RVE** of the **SFFRC** is

$$V_{\text{CNT}}|_{\max} = \frac{V^{\text{CNT}}}{V^{\text{SFFRC}}} = \frac{\pi d_n^2}{2\left(d_n + 1.7 \times 10^{-9}\right)^2} \left(\sqrt{\frac{\pi V_p}{2\sqrt{3}}} - V_p \right) \tag{5.44}$$

Finally, the maximum volume fraction ($V_{nt}|_{\max}$) of the **CNT**s with respect to the volume of the **PMNC** can be determined as follows:

$$V_{nt}|_{\max} = \frac{V^{\text{CNT}}}{V^{\text{PMNC}}} = \frac{2\sqrt{3}}{\pi - 2\sqrt{3} V_p} V_{\text{CNT}}|_{\max} \tag{5.45}$$

5.6 Numerical Example

An example of the **SFFRC** is considered for presenting the numerical estimation of its effective properties. The **SFFRC** considered here is composed of epoxy, **PZT5** fiber, and armchair **CNT**s. The material properties of these constituent phases are listed in Table 5.1.

It is evident from Eq. (5.39) that when V_p is zero, V_{CNT} is zero. Also, when $V_p = \pi/2\sqrt{3}$, i.e., **PMNC** is absent, the value of V_{CNT} is also zero. Thus, the maximum value of V_{CNT} given by Eq. (5.39) will be maximized at a particular value of V_p. Figure 5.9 illustrates the variation of the maximum volume fraction of

Table 5.1 Material properties of the constituent phases of **SFFRC**

Material	C_{11} (GPa)	C_{12} (GPa)	C_{23} (GPa)	C_{33} (GPa)	C_{55} (GPa)	e_{31} (Cm^{-2})	e_{33} (Cm^{-2})	(nm)
CNT (5, 5) Shen and Li (2004)	2143.4	184.4	404	668	791	–	–	$d_n = 0.678$
CNT (10, 10) Shen and Li (2004)	1088.4	87.8	254		442	–	–	$d_n = 1.356$
CNT (20, 20) Shen and Li (2004)	545	43.52	134	138	227	–	–	$d_n = 2.712$
PZT5 Smith and Auld (1991)	121	75.4	75.2	111	21.1	−5.4	15.8	–
Epoxy Smith and Auld (1991)	5.3	3.1	3.1	5.3	0.64	–	–	–

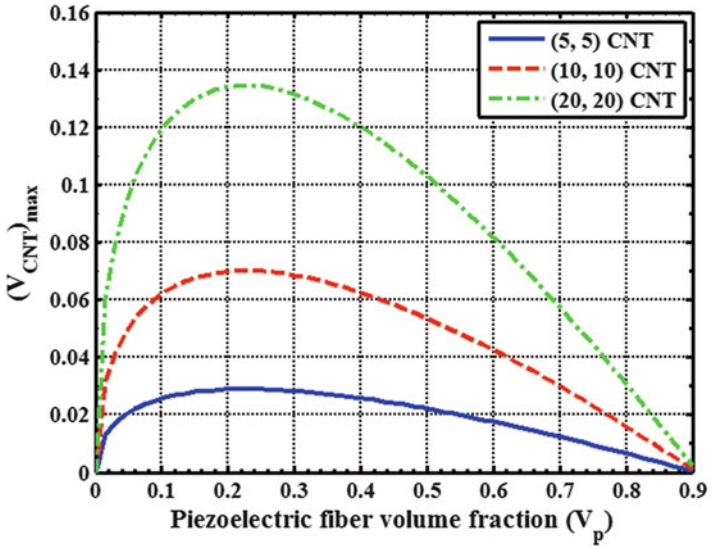

Fig. 5.9 Variation of the maximum value of **CNT** volume fraction with the piezoelectric fiber volume fraction in **SFFRC**

CNTs in the **SFFRC** with respect to V_p. It may be observed from this figure that the maximum values of V_{CNT} for different **CNT** diameters are almost independent of the **CNT** diameter and are maximized at $V_p = 0.24$. Few graphical results are presented in Figs. 5.10, 5.11, 5.12, 5.13, and 5.14. While estimating the effective properties shown in Figs. 5.10, 5.11, 5.12, 5.13, and 5.14, the maximum value of

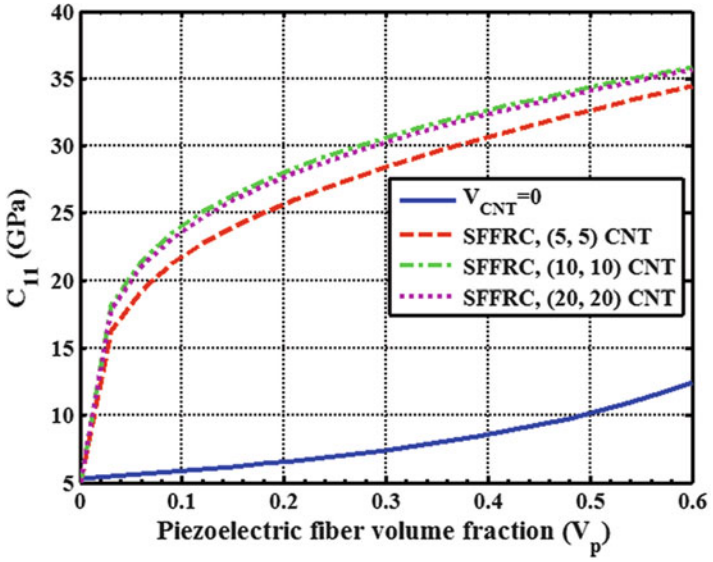

Fig. 5.10 Effective elastic coefficient C_{11} of the **SFFRC**

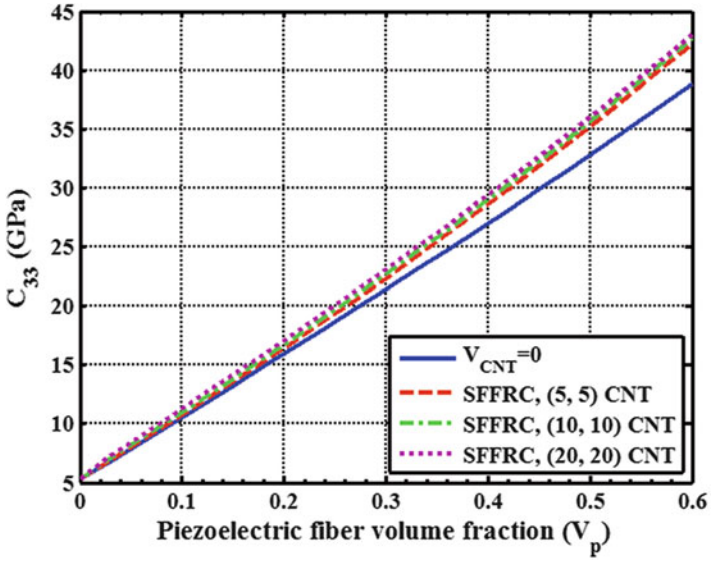

Fig. 5.11 Effective elastic coefficient C_{33} of the **SFFRC**

V_{CNT} for a particular value of V_p is used from Eq. (5.39). First the effective properties of the **PMNC** are computed using Eq. (5.23). Using the results obtained by Eq. (5.23), effective properties of the **PCFF** are evaluated from Eqs. (5.26) and

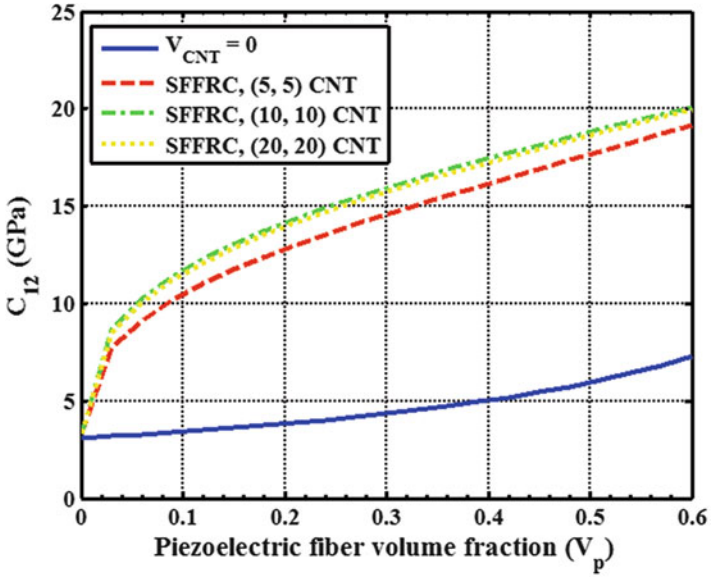

Fig. 5.12 Effective elastic coefficient C_{12} of the **PFFRC**

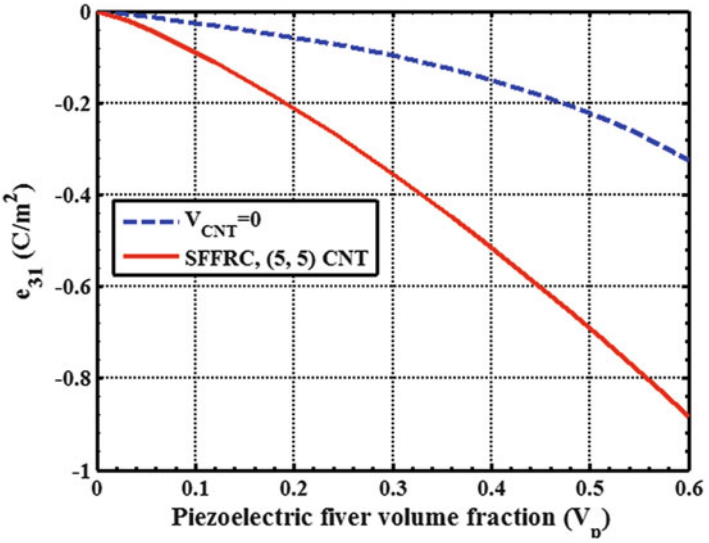

Fig. 5.13 Effective in-plane piezoelectric coefficient e_{31} of the **SFFRC**

(5.27). Finally, Eqs. (5.30) and (5.31) are used to estimate the effective properties of the **SFFRC**. Figure 5.10 illustrates the variation of the effective in-plane elastic coefficient C_{11} of the **SFFRC** with the piezoelectric fiber volume fraction V_p. It

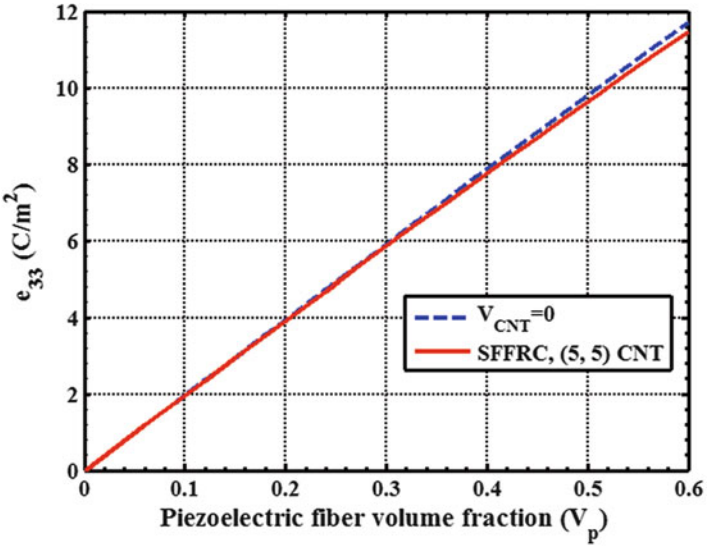

Fig. 5.14 Effective piezoelectric coefficient (e_{33}) of the **SFFRC**

may be observed from Fig. 5.10 that the effective value of C_{11} of the **PFFRC** is significantly larger than that of the existing 1–3 **PZC** without having **CNT**s.

This is attributed to the fact that the radially grown **CNT**s strengthen the matrix surrounding the piezoelectric fiber along 1- or 1′-direction. Figure 5.11 illustrates the variation of the transverse effective elastic coefficient C_{33} of the **SFFRC** with the piezoelectric fiber volume fraction V_p. It is important to note from this figure that the radially grown **CNT**s on the surface of the piezoelectric fibers do not appreciably affect the magnitude of the effective transverse elastic coefficient C_{33} when compared with that of the existing 1–3 **PZC** without **CNTs**. This is attributed to the fact that the **CNT**s are grown transverse to the piezoelectric fiber and the elastic properties of **CNT** transverse to its axis (i.e., along 3-direction) are much less than those along its axis. Radially grown **CNT**s also significantly improve the other effective elastic coefficient C_{12} of the **SFFRC** as shown in Fig. 5.12. It is also to be noted from Figs. 5.10, 5.11, and 5.12 that the **CNT** diameter marginally influences the effective elastic properties of the **SFFRC**. Figure 5.13 illustrates the variation of the effective in-plane piezoelectric coefficient e_{31} of the **SFFRC**. It can be observed from this figure that for $V_p = 0.6$, the magnitude of e_{31} of the **SFFRC** is almost three times that of the existing 1–3 **PZC** without containing **CNT**s. This enhancement of the in-plane piezoelectric coefficient is attributed to the in-plane stiffening of the polymer matrix surrounding the piezoelectric fiber by radially grown aligned **CNT**s. The other in-plane effective piezoelectric coefficient e_{32} is found to be identical to e_{31}. It is because that the **SFFRC** is transversely isotropic. Figure 5.14 illustrates the variation of the effective transverse piezoelectric coefficient e_{33} of the **SFFRC** with the piezoelectric fiber volume fraction. It is important

to note from this figure that the radially grown **CNT**s on the surface of the piezoelectric fibers negligibly affect the magnitude of the effective piezoelectric coefficient e_{33} when compared with that of the 1–3 **PZC** without **CNT**s.

References

Aboudi, J., Arnold, S.M., Bednarcyk, B.A.: Micromechanics of composite materials. Academic Press, New York (2013)

Bailey, T., Hubbard, J.E.: Distributed piezoelectric polymer active vibration control of a cantilever beam. AIAA J. Guid. Contr. **8**, 605–611 (1985)

Baz, A., Poh, S.: Performance of an active control system with piezoelectric actuators. J. Sound Vib. **126**, 327–343 (1988)

Bower, C., Zhu, W., Jin, S., Zhou, O.: Plasma-induced alignment of carbon nanotubes. Appl. Phys. Lett. **77**, 830–832 (2000)

Bruke, S.E., Hubbard, J.E.: Active vibration control of a simply supported beam using a spatially distributed actuator. IEEE Contr. Syst. Mag. **8**, 25–30 (1987)

Chatzigeorgiou, G., Seidel, G.D., Lagoudas, D.C.: Effective mechanical properties of fuzzy fiber composites. Compos. B **43**, 2577–2593 (2012)

Chee, C., Tong, L., Steven, G.P.: Piezoelectric actuator orientation optimization for static shape control of composite plates. Compos. Struct. **55**, 169–184 (1999)

Cheng, H.C., Liu, Y.L., Hsu, Y.C., Chen, W.H.: Atomistic-continuum modeling for mechanical properties of single-walled carbon nanotubes. Int. J. Solid. Struct. **46**, 1695–1704 (2009)

Crawley, E.F., Luis, J.D.: Use of piezoelectric actuators as elements of ontelligent structures. AIAA J. **27**, 1801–1807 (1987)

Dhala, S., Ray, M.C.: Micromechanics of piezoelectric fuzzy fiber-reinforced composites. Mech. Mater. **81**, 1–17 (2015)

Forward, R.L.: Electronic damping of orthogonal bending modes in a cylindrical mast-experiment. J. Spacecraft Rocket. **18**, 11–17 (1981)

Gao, X.L., Li, K.: A shear-lag model for carbon nanotube reinforced polymer composites. Int. J. Solid. Struct. **42**, 1649–1667 (2005)

Gracia, E.J., Wardle, B.L., Hart, A.J., Yamamoto, N.: Fabrication and multifunctional properties of a hybrid laminate with aligned carbon nanotubes grown in situ. Compos. Sci. Technol. **68**, 2034–2041 (2008)

Griebel, M., Hamaekers, J.: Molecular dynamics simulations of the elastic moduli of polymer–carbon nanotube composites. Comput. Meth. Appl. Mech. Eng. **193**, 1773–1788 (2004)

Ha, S.K., Keilers, C., Chang, F.K.: Finite element analysis of composite structures containing distributed piezoceramic sensors and actuators. AIAA J. **30**, 772–780 (1992)

Iijima, S.: Helical microtubules of graphitic carbon. Nature **354**, 56–58 (1991)

Im, S., Atluri, S.N.: Effects of piezoactuator on a finitely deformed beam subjected to general loading. AIAA J. **25**, 1373–1385 (1989)

Jiang, B., Liu, C., Zhang, C., Liang, R., Wang, B.: Maximum nanotube volume fraction and its effect on overall elastic properties of nanotube-reinforced composites. Composites B **40**, 212–217 (2009)

Kundalwal, S.I., Ray, M.C.: Micromechanical analysis of fuzzy fiber reinforced composites. Int. J. Mech. Mater. Des. **7**, 149–166 (2011)

Kundalwal, S.I., Ray, M.C.: Effective properties of a novel composite reinforced with short carbon fibers and radially aligned carbon nanotubes. Mech. Mater. **53**, 47–60 (2012)

Lanzara, G., Chang, F.K.: Design and characterization of a carbon-nanotube-reinforced adhesive coating for piezoelectric ceramic discs. Smart Mater. Struct. **18**, 125001 (2009)

Lin, C., Hsu, C., Huang, H.N.: Finite element analysis on deflection control of plates with piezoelectric actuators. Compos. Struct. **35**, 423–433 (1996)
Mathur, R.B., Chatterjee, S., Singh, B.P.: Growth of carbon nanotubes on carbon fiber substrates to produce hybrid/phenolic composites with improved mechanical properties. Compos. Sci. Technol. **68**, 1608–1615 (2008)
Miller, S.E., Hubbard, J.E.: Observability of a Bernoulli-Euler beam using PVF2 as a distributed sensor. MIT Draper Laboratory Report (1987)
Newnham, R.E., Shinner, D.P., Cross, L.E.: Connectivity and piezoelectric-pyroelectric composites. Mater. Res. Bull. **13**, 525–536 (1978)
Odegard, G.M., Gates, T.S., Wise, K.E., Park, C., Siochi, E.J.: Constitutive modeling of nanotube-reinforced polymer composites. Compos. Sci. Technol. **63**, 1671–1687 (2003)
Ray, M.C.: Concept of a novel hybrid smart composite reinforced with radially aligned zigzag carbon nanotubes on piezoelectric fibers. Smart Mater. Struct. **19**, 035008 (2010)
Ray, M.C., Faye, A.: Theoretical and experimental investigations on active structural-acoustic control of thin isotropic plate using vertically reinforced 1-3 piezoelectric composite. Smart Mater. Struct. **18**, 015012 (2009)
Ray, M.C., Pradhan, A.K.: On the use of vertically reinforced 1-3 piezoelectric composites for hybrid damping of laminated composite plates. Mech. Adv. Mater. Struct. **15**, 245–261 (2007)
Ray, M.C., Bhattacharyya, R., Samanta, B.: Static analysis of an intelligent structure by the finite element method. Comput. Struct. **52**, 617–631 (1994)
Saravanos, D.A., Hetliger, P.R., Hopkins, D.A.: Layerwise mechanics and finite element for the dynamic analysis of piezoelectric composite plates. Int. J. Solid. Struct. **34**, 359–378 (1997)
Seidel, G.D., Lagoudas, D.C.: Micromechanical analysis of the effective elastic properties of carbon nanotube reinforced composites. Mech. Mater. **38**, 884–907 (2004)
Shadlou, M.R., Shokrieh, S., Ayatollahi, M.M.: Multiscale modeling for mechanical properties of carbon nanotube reinforced nanocomposites subjected to different types of loading. Compos. Struct. **93**, 2250–2259 (2011)
Shen, L., Li, J.: Transversely isotropic elastic properties of single-walled carbon nanotubes. Phys. Rev. B **69**, 045414 (2004)
Smith, W.A., Auld, B.A.: Modeling 1-3 composite piezoelectrics: thickness mode oscillations. IEEE Trans. Ultrason. Ferroelectr. Freq. Control **31**, 40–47 (1991)
Sohn, J.W., Choi, S.B., Lee, C.H.: Active vibration control of smart hull structure using piezoelectric actuator. Smart Mater. Struct. **18**, 074004 (2009)
Suresh Kumar, R., Ray, M.C.: Active control of geometrically nonlinear vibrations of doubly curved smart sandwich shells using 1-3 piezoelectric composites. Compos. Struct. **105**, 173–187 (2012)
Thostenson, E.T., Chou, T.W.: On the elastic properties of carbon nanotubes based composites: modelling and characterization. J. Phys. D Appl. Phys. **36**, 573–582 (2003)
Treacy, M.M.J., Ebbessen, T.W., Gibson, J.M.: A Exceptionally high Young's modulus observed for individual carbon nanotube. Nature **381**, 678–680 (1996)
Varadarajan, S., Chandrashekhara, K., Agarwal, S.: LQG/LTR-based robust control of composite beams with piezoelectric devices. J. Vib. Control. **6**, 607–630 (2000)
Zhang, Q., Qian, W., Xiang, R., Yang, Z., Luo, G., Wang, Y., Wei, F.: In situ growth of carbon nanotubes on inorganic fibers with different surface properties. Mater. Chem. Phys. **107**, 317–321 (2008)